surfaces

MDPI

Article

Optical Characteristics of Directly Deposited Gold Nanoparticle Films

Jordi Sancho Parramon [1], Tilen Švarc [2], Peter Majerič [2,3], Žiga Jelen [2,4] and Rebeka Rudolf [2,3,4,*]

[1] Institut Ruđer Bošković, Bijenička cesta 54, 10000 Zagreb, Croatia; jsancho@irb.hr
[2] Faculty of Mechanical Engineering, University of Maribor, Smetanova ulica 17, 2000 Maribor, Slovenia; tilen.svarc1@um.si (T.Š.); peter.majeric@um.si (P.M.); z.jelen@um.si (Ž.J.)
[3] Zlatarna Celje d.o.o., Kersnikova ulica 19, 3000 Celje, Slovenia
[4] Pomurje Science and Innovation Centre, Lendavska ulica 5a, 9000 Murska Sobota, Slovenia
* Correspondence: rebeka.rudolf@um.si

Abstract: The manuscript presents the optical properties of directly deposited films of gold nanoparticles (AuNPs) prepared by the Ultrasonic Spray Pyrolysis (USP) technology. Four samples were produced, with AuNP deposition times on the glass substrate of 15 min, 30 min, 1 h and 4 h. The morphological characterisation of the deposited films showed that the size of the first deposited AuNPs was between 10 and 30 nm, while, with a longer duration of the deposition process, larger clusters of AuNPs grew by coalescence and aggregation. The prepared layers were characterised optically with Ultraviolet–visible spectroscopy (UV–vis) and ellipsometry. The ellipsometric measurements showed an increasingly denser and thicker effective thickness of the AuNP layers. The extinction spectra displayed a clear local surface plasmonic resonance (LSPR) signature (peak 520–540 nm), indicating the presence of isolated particles in all the samples. For all AuNP layers, the imaginary part of the parallel and perpendicular components of the anisotropic dielectric function was dominated by a central peak at around 2.2 eV, corresponding to the LSPR of isolated particles, and a high-energy shoulder due to Au interband transitions. It was shown that, as the density of particles increased, the extinction cross-section grew over the whole spectral range where measurements are taken. Thus, the response can be explained with an enhanced electromagnetic response between the AuNPs that can be connected to the increase in particle density, but also by the formation of clusters and irregular structures.

Keywords: optical characteristics; gold nanoparticles' films; UV–vis; ellipsometry measurements

Citation: Parramon, J.S.; Švarc, T.; Majerič, P.; Jelen, Ž.; Rudolf, R. Optical Characteristics of Directly Deposited Gold Nanoparticle Films. *Surfaces* **2024**, *7*, 369–379. https://doi.org/10.3390/surfaces7020023

Academic Editor: Mattia Cattelan

Received: 19 March 2024
Revised: 18 April 2024
Accepted: 15 May 2024
Published: 27 May 2024

1. Introduction

Gold nanoparticles (AuNPs) were utilised due to their exceptional chemical and physical properties, with a particular emphasis on their fascinating optical characteristics arising from local surface plasmonic resonance (LSPR) [1–3]. LSPR is the occurrence of a resonance of the incident electromagnetic field and the plasmon of a particle, which occurs when the frequency of the electromagnetic field is equal to the inherent frequency of oscillation of the cloud of free electrons within the particle. As a result of this resonance, the electronic cloud is excited, generating its own electric field that influences the absorption and scattering of light [4,5].

Thin layers of metallic materials undergo propagating surface plasmon resonance (PSPR), where the plasmon propagates along the surface of the film layer. PSPRs exhibit a continuous dispersion relation, enabling their existence across a broad spectrum of frequencies [6]. In contrast, LSPRs are confined to a finite frequency range, due to the constraints imposed by their finite dimensions. The spectral positioning of LSPR is dictated by factors such as the particle's size and shape, along with the dielectric properties of both the metal and the surrounding medium [4–6]. Notably, LSPR can undergo direct coupling with propagating light, a capability not shared by PSPRs.

In the case of copper, silver and gold, LSPR occurs in the visible light range [4,7]. Therefore, these metallic elements are particularly appealing for optical applications, as they enable controlled manipulation of the light's properties. Additionally, gold has a high ionisation potential, and is therefore highly resistant to oxidation and corrosion. This makes it applicable for use in various media and environments, in various biological or chemical conditions, as well as in electronic or aerospace settings, which may not be considered suitable for less corrosion-resistant materials. The occurrence of LSPR opens doors to numerous applications, where the unique optical characteristics of these noble metal nanoparticles can be exploited, such as in sensors [8–12], biomedical applications [13–18], advanced optical materials [17,19], where the corrosion resistance of gold is important for signal transmission and monitoring of physical quantities, or photocatalysis [20,21].

The Mie theory allows for the prediction of LSPR in particles. For spherical particles, there are simplified numerical models that assume various oscillations of the electronic cloud known as discrete dipole approximation (DDA), such as dipole and quadrupole oscillations [4]. The analytical calculation of LSPR is feasible for spherical particles [3,22], whereas complex particle shapes require complex numerical solutions [4,23].

Analytical and numerical calculations offer a good prediction of the absorption peaks of nanoparticle suspensions, since nanoparticles undergo Brownian motion [5,24,25] and are in contact with other particles for an insignificant amount of time, if any at all, due to the presence of repulsive forces or steric stabilisers. Steric stabilisers are added to nanoparticles' suspensions to stabilise the solution and prevent agglomeration and aggregation when the repulsive forces are not sufficient [5,26,27]. Stabilisers can also prevent agglomeration and aggregation of nanoparticles, while removing the dispersion media slowly [28–30]. Without the presence of stabilisers, the nanoparticles agglomerate and aggregate during the removal of the dispersion media, which changes the colour of the gold nanoparticles directly. A similar phenomenon is expected when AuNPs are layered on each other with direct deposition within the reaction chamber of an ultrasound spray pyrolysis (USP) device. No sintering is expected to occur, since the temperatures inside the USP device in the deposition zone are not near the sintering temperature of the AuNPs [30]. No direct deposition of AuNPs from an USP process has been observed in the available literature, as this process is used mainly for the production of discrete nanoparticles. Therefore, this research work aims to characterise the optical properties of an AuNPs film prepared by this technology, in order to evaluate the possibility of using USP for coating of the Au layers. This process has a continuous operation for nanoparticle production, which could be used for a high output of Au coatings on glass substrates, if a successful coating is feasible. Overall, the investigated samples displayed narrow-sized distributions, with spectral optical responses essentially defined by the plasmon resonance of isolated particles. At the same time, the magnitude of optical extinction was controlled by the density of particles, regulated by the deposition time. This feature evidences the advantage of the fabrication method in comparison to other bottom-up approaches, in which the morphology, and, hence, optical properties are hard to control.

2. Materials and Methods

2.1. Gold Nanoparticle Synthesis and Gold Nanoparticle Film Preparation

A USP process was used for producing the AuNPs layer on the glass substrate (Figure 1). The precursor used was Hydrogen tetrachloroaurate (III) trihydrate ($HAuCl_4 \cdot 3H_2O$, molecular weight: 393.83 g/mol, Glentham Life Sciences, UK), dissolved in deionised water at a concentration of 0.5 g/L Au (1.0 g/L $HAuCl_4 \cdot 3H_2O$; Au with a molar weight of 196.967 g/mol represents 50% of the weight of Hydrogen tetrachloroaurate (III) trihydrate). The USP process was carried out using a proprietary device from Zlatarna Celje d.o.o., Slovenia [30], consisting of a custom built tube furnace, an ultrasonic generator, a precursor supply system, and a gas washing system for nanoparticle collection. The ultrasonic generator is constructed with a 1.6 MHz piezoceramic membrane for generating the ultrasound (Liquifog II, Johnson Matthey Piezo Products GmbH, Germany), which is submerged in

a chamber for the aerosolization of the precursor solution. The generated precursor mist is transported in the tube furnace with nitrogen gas at a rate of 6 L/min. The quartz tube furnace has three heating zones, with a length of 400 mm each and an internal diameter of 35 mm. The tube furnace heating zone temperatures were set at 200, 400 and 400 °C. The hydrogen gas was introduced into the tube between the first and second heating zones at a rate of 6 L/min. The borosilicate glass substrate (Duran Borosilicate glass 3.3 according to ISO 3585, DWK Life Sciences GmbH, Mainz, Germany), with dimensions of 1.5 × 2.5 cm and a thickness of 1 mm, was positioned inside the reaction tube at an angle of 45°, about 10 cm from the end of the third heating zone. The glass substrate was cleaned with ethanol before use, in order to remove any dust or residues before deposition. The precursor droplets inside the tube furnace undergo droplet evaporation and shrinkage, diffusion of the hydrogen tetrachloroaurate to the droplet centre, reduction with hydrogen gas and final nanoparticle densification, before hitting and depositing a layer of AuNPs on the substrate. Four samples were produced, with AuNP deposition times of 15 min, 30 min, 1 h and 4 h on the glass substrate.

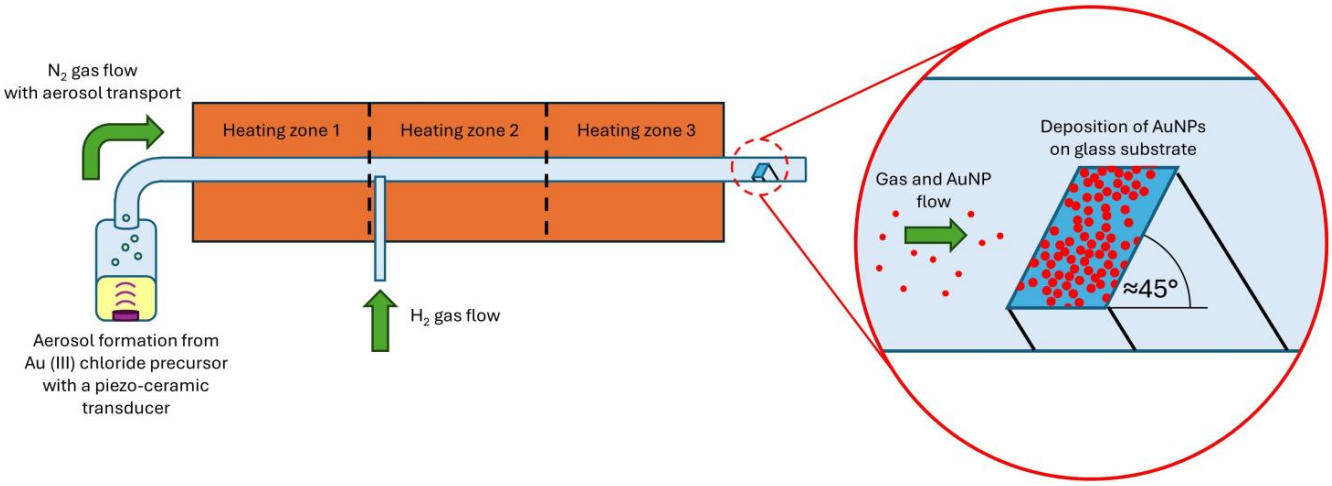

Figure 1. Deposition of AuNPs on the glass substrate with the USP process.

2.2. Morphological Characterisation

A Scanning Electron Microscope, Sirion 400 NC SEM (FEI, Hillsboro, OR, USA), was used for the surface investigations of the prepared layer of AuNPs on the glass substrate. The SEM was equipped with an INCA 350 EDS detector (Oxford Instruments, Abingdon, Oxfordshire, UK) for microchemical analysis. The glass substrates with deposited AuNPs from the USP were coated with carbon, for providing sufficient conductivity for the SEM imaging and EDS analysis. Particle sizes were measured with SEM software and ImageJ (version 1.54h), with at least 500 particles measured for a given sample.

2.3. Optical Characterisation

The prepared layers were characterised optically with Ultraviolet–visible spectroscopy (UV–vis) and ellipsometry.

The UV–vis measurements were performed with a Tecan Infinite M200 (Tecan Group Ltd., Männedorf, Switzerland) UV–Vis spectrophotometer, by inserting the sample plates into the light beam path with the following parameters: absorbance range: λ = 400 to 700 nm, no. flashes: 5×.

The samples were investigated by spectroscopic ellipsometry measurements in the spectral range between 0.57 and 3.5 eV with a V-VASE ellipsometer (J.A. Woollam, Lincoln, NE, USA), at incidences of 45°, 55° and 65°. The transmittance measurements at the normal incidence were taken at the same sample point, to increase the reliability of the characterisation results [31]. In order to fit the experimental measurements, the layer of gold nanoparticles was modelled using an effective medium approach, i.e., the layer was

treated as a homogeneous film, with its optical response completely determined by its effective thickness and effective optical constants. The effective optical constants were modelled using a multiple oscillator model that can take into account the LSPR of the AuNPs and Au interband transitions in the high energy range, as described elsewhere [32]. Data fitting was conducted by optimising the parameters describing the sample model through the minimisation of a figure of merit that quantifies the discrepancy between the simulated and experimental data.

3. Results

3.1. Morphological Characterisation

A detailed SEM examination of the samples showed AuNPs deposited in a discontinuous layer across the samples' surfaces (Figure 2). The number of AuNPs was the lowest for the sample with 15 min of deposition, and increased as more time was given for deposition on the glass substrate. As expected, the sample with 4 h of deposition had the highest number of AuNPs, while the nanoparticle sizes were also the biggest for this sample.

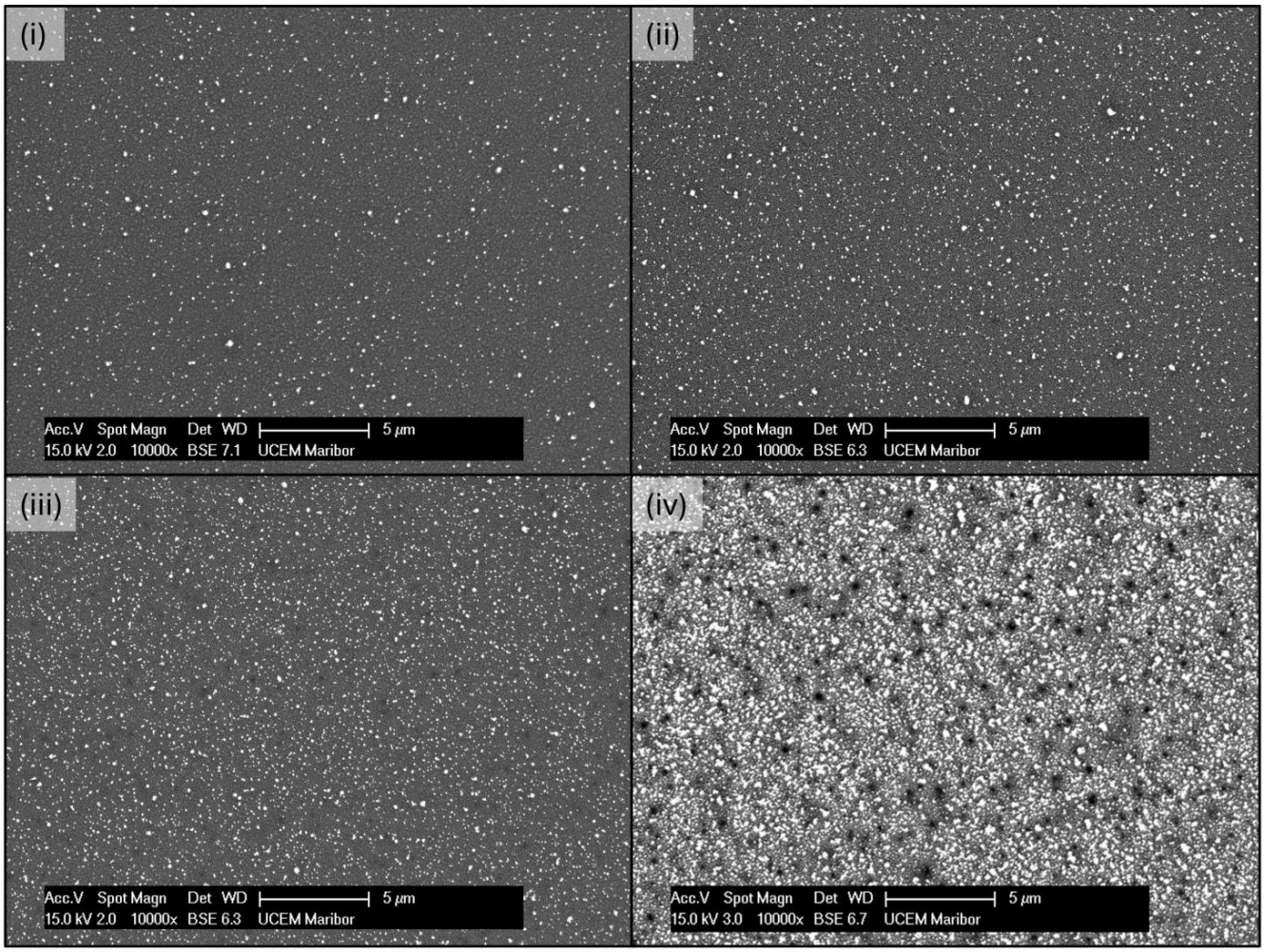

Figure 2. Low magnification SEM images of the samples with USP deposition of AuNPs for (**i**) 15 min, (**ii**) 30 min, (**iii**) 1 h and (**iv**) 4 h, showing the nanoparticle coverage on the glass substrate.

The differences between nanoparticle sizes and shapes can be seen in Figure 3. Larger particles were produced as more time was given to the AuNPs' deposition. The AuNPs with 15 min deposition were small, with measured sizes from 10–30 nm, with individual nanoparticles that were somewhat larger, mostly around 60–120 nm. An example of nanoparticle measurements of the sample with 1 h deposition is presented in Figure 4. The smaller nanoparticles were spherical in shape. As the nanoparticle size increased, they

became increasingly more irregular in shape. With longer deposition times (30 min and 1 h), an increasingly higher number of larger nanoparticles (around 100 nm and up to 200 nm) were present, while the smaller 10–30 nm nanoparticles were still dominating in number. With the longest deposition time of 4 h, the larger particles were more numerous and prevalent on the sample surface as compared to the previous samples. In this sample, the larger, irregularly shaped particles and clusters of these particles were measured up to a value of 380 nm. Therefore, larger deposition times are not reported here, because they resulted in broad and inhomogeneous particle sizes and shape distributions, widening, and quenching the well-defined plasmon resonances of small, isolated particles. There were also dark spots present on the sample's surface (Figures 2iv and 3iv), where nanoparticles were not present, or only very small nanoparticles around 10 nm were present in lower numbers.

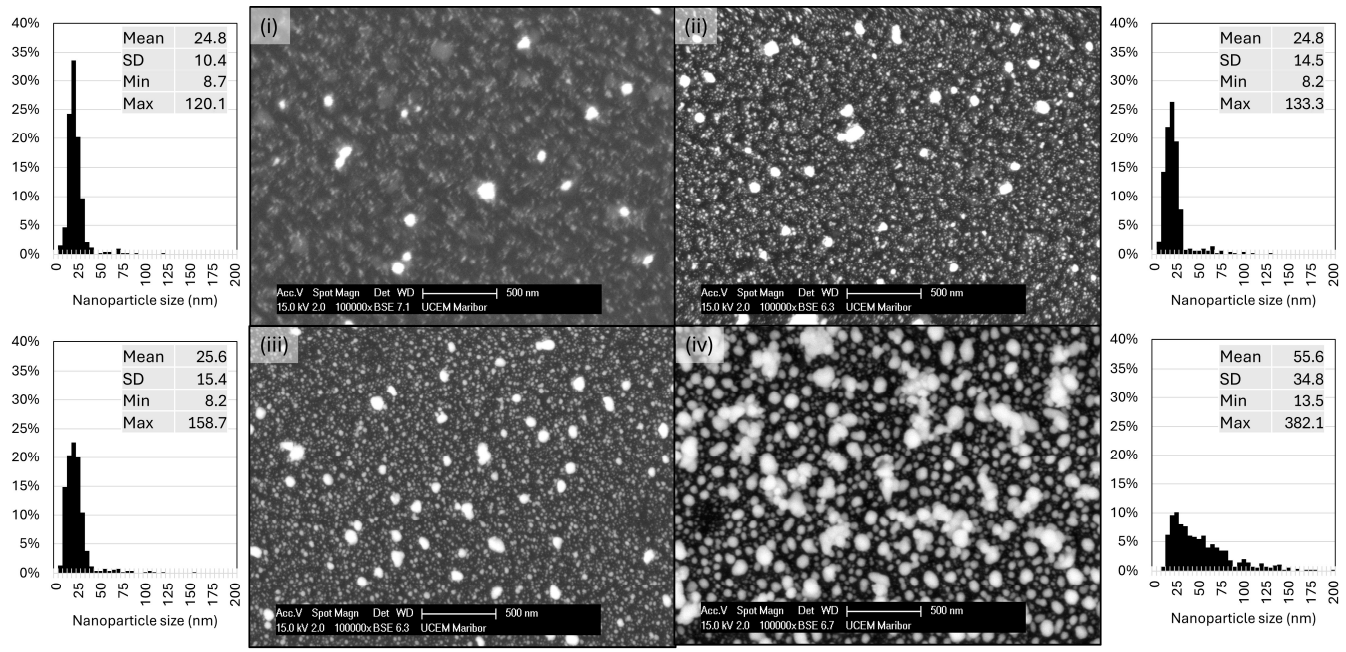

Figure 3. High magnification SEM images of the samples with USP deposition of AuNPs for (**i**) 15 min, (**ii**) 30 min, (**iii**) 1 h and (**iv**) 4 h, showing the nanoparticles' morphology. Particle size histograms are included for each deposition time, with calculated mean, Standard Deviation, minimum and maximum values from the SEM image measurements.

The EDX analysis of the samples showed the presence of Au, along with elements which were constituents of the glass substrate—Si, O and minor elements of Na, Mg, Ca, Al. The interaction volume of a few µm, from which X-rays are emitted during the EDS analysis, was much larger than the AuNPs' sizes, resulting in the detection of the glass substrate elements, along with the AuNPs. More importantly, no Cl or other impurities were detected in the samples, which would indicate an incomplete synthesis of the nanoparticles from the chloride precursor, or contamination from other elements during the synthesis and deposition of the AuNPs. An example of the EDX analysis for a sample with 1 h of AuNPs' deposition is shown in Figure 4; the other samples had similar results.

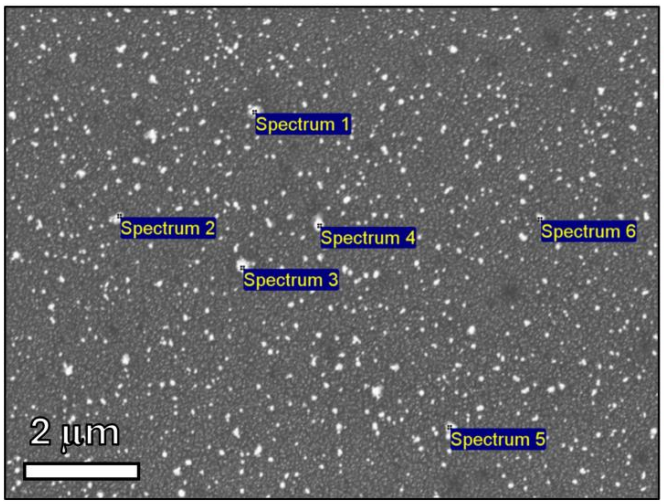

Spectrum	O	Na	Mg	Al	Si	Ca	Au	Total
Spectrum 1	50.77	7.07	2.41	0.59	28.37	3.08	7.70	100.00
Spectrum 2	51.86	7.10	2.07	0.63	29.01	2.70	6.63	100.00
Spectrum 3	47.57	6.79	2.07	0.60	28.15	3.13	11.70	100.00
Spectrum 4	49.47	7.04	2.09	0.69	30.21	2.60	7.88	100.00
Spectrum 5	48.55	6.74	2.03	0.53	27.78	2.42	11.95	100.00
Spectrum 6	51.24	7.35	2.21	0.68	28.94	2.81	6.77	100.00
Mean	**49.91**	**7.02**	**2.15**	**0.62**	**28.74**	**2.79**	**8.77**	**100.00**
Std. Dev.	**1.67**	**0.22**	**0.14**	**0.06**	**0.86**	**0.28**	**2.42**	
Max.	**51.86**	**7.35**	**2.41**	**0.69**	**30.21**	**3.13**	**11.95**	
Min.	**47.57**	**6.74**	**2.03**	**0.53**	**27.78**	**2.42**	**6.63**	

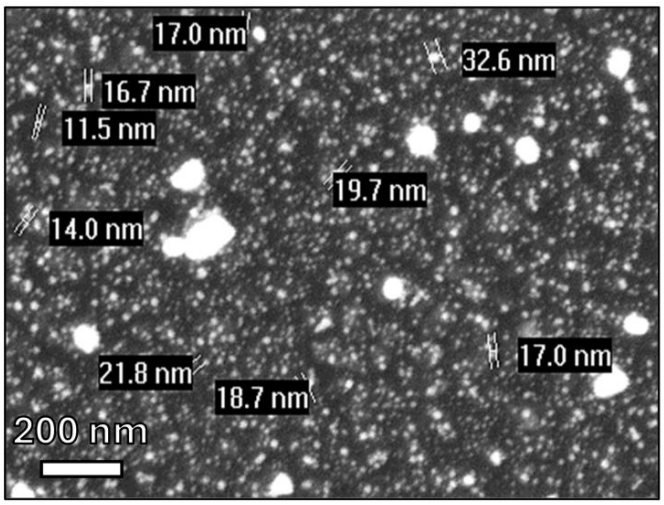

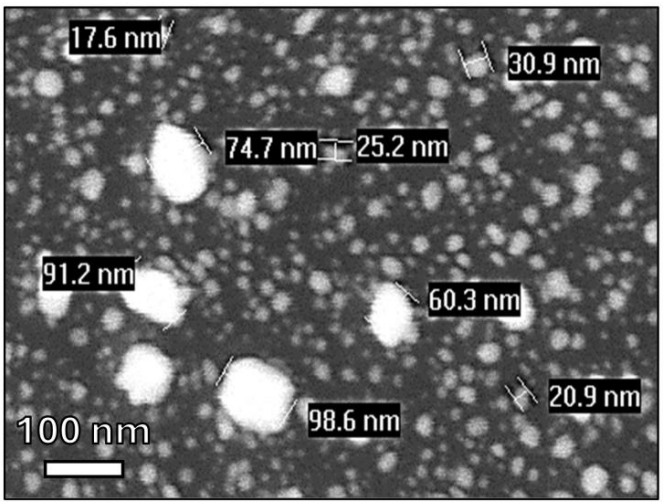

Figure 4. EDX analysis and particle size measurements for the sample with 1 h of AuNP deposition.

3.2. Optical Characterisation

The extinction spectra of the samples with USP deposition for 15 min, 30 min, 1 h and 4 h are shown in Figure 5. The spectra display a clear LSPR signature (peak 520–540 nm), indicating the presence of isolated particles in all the samples. The strength of the extinction peak rose with the deposition time, accounting for the increase in the number of deposited particles. In addition to the LSPR peak, the larger deposition times resulted in a progressive increase in extinction in the long-wavelength range, that might be explained by electromagnetic interaction between the particles and the presence of larger/clustered particles, as discussed in Section 4.

In the first step, the ellipsometric measurements were fitted using an isotropic model for the effective optical constants of the AuNPs' layer, leading to a fair agreement with the experimental data, with the multiple oscillator model providing better data fits than the Maxwell-Garnett effective medium theory [33]. A significantly better agreement was obtained if the AuNP film was modelled as a uniaxial anisotropic layer, with different effective dielectric functions for light polarised along the plane parallel ($\varepsilon//$) or perpendicular ($\varepsilon\perp$) to the sample's surface. As an example, the experimental data fits for the sample obtained for 30 min deposition are shown in Figure 6i–iii. The measurements for the sample obtained after 4 h deposition showed very large depolarisation values, probably due to large scattering, and it was not possible to fit them with the current model.

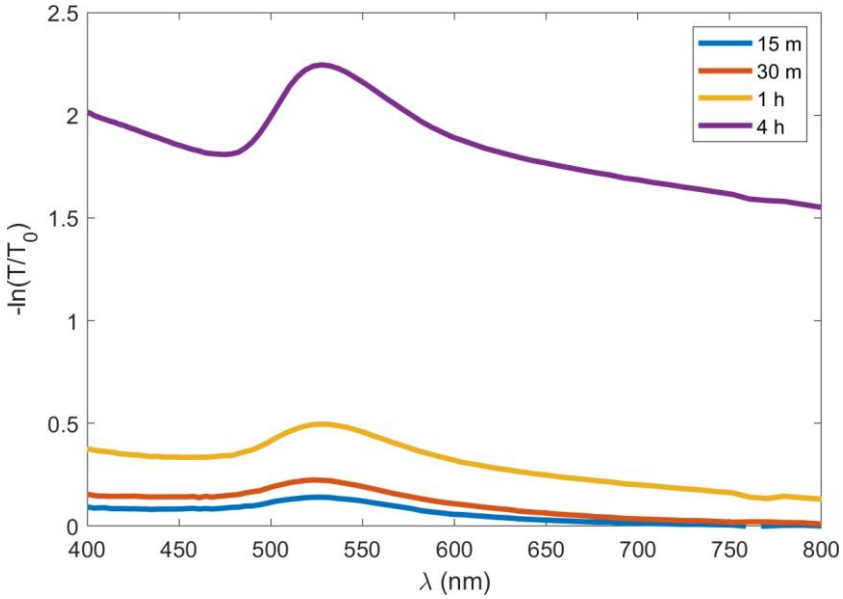

Figure 5. Extinction spectra calculated from the transmittance of the bare (T_0) and coated (T) substrate for different deposition times.

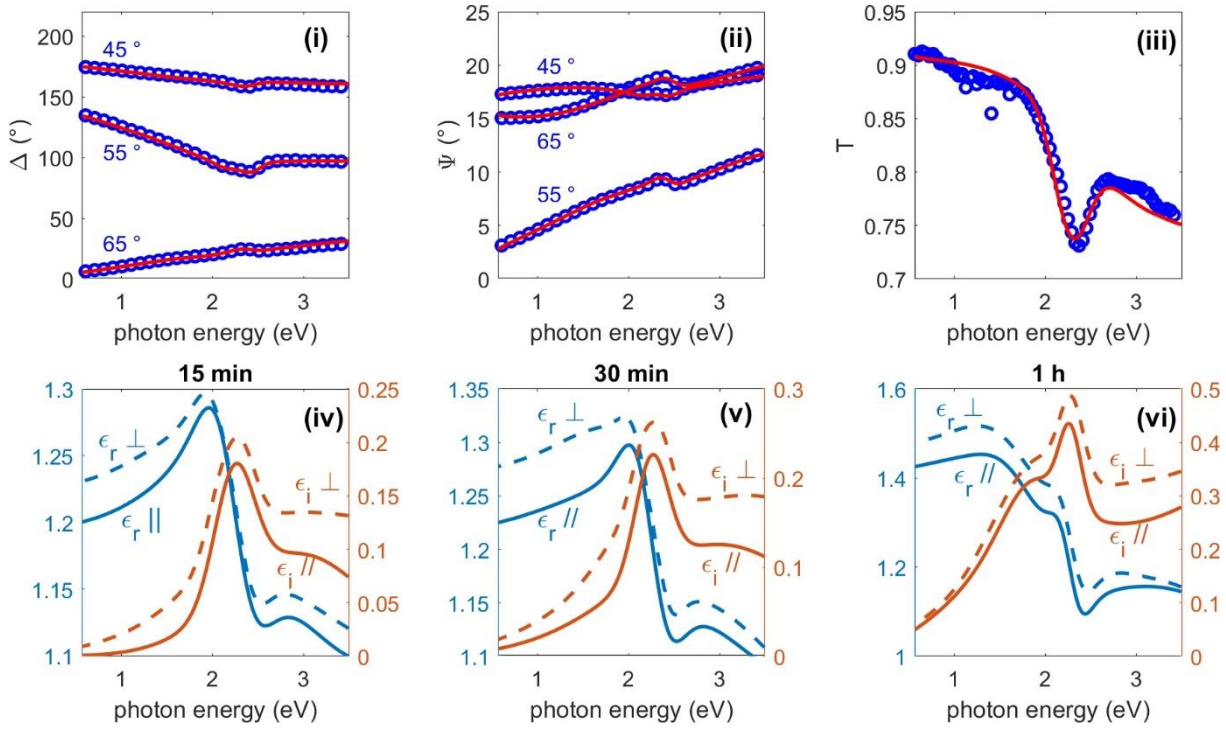

Figure 6. Top panel: Fits of the ellipsometric angles Δ (**i**), Ψ (**ii**) and transmittance (**iii**) spectra for the sample deposited for 30 min. The experimental data are shown by the dots and the fit by the solid lines. The annotated numbers in the Δ and Ψ spectra indicate the angle of incidence. Bottom panel: The real (εr) and imaginary (εi) parts of the effective dielectric function of the AuNP layer deposited for 15 min (**iv**), 30 min (**v**) and 1 h (**vi**), for both in-plane (ε//) and out of plane (ε⊥) components, i.e., for light polarised parallel and perpendicular to the sample plane.

For all the AuNP layers, the imaginary part of both ε//and ε⊥ was dominated by a central peak around 2.2 eV, corresponding to the LSPR of isolated particles, and a high-energy shoulder due to Au interband transitions. It should be noted that the LSPR peak became broader and more intense for longer deposition times, which can be explained

by a larger concentration of nanoparticles in the AuNP layer that gave place to stronger interparticle electromagnetic interactions [34]. In general, both the real and imaginary parts of $\varepsilon\perp$ displayed larger values than $\varepsilon//$, which can be explained by the larger polarizability of the particle when light is polarised perpendicularly to the sample surface due to the presence of the substrate and the resulting image effects [35].

Finally, the effective thickness of the AuNP layer for samples deposited at 15, 30 and 60 min were 79, 97 and 110 nm, suggesting that, as the deposition time increased, the AuNP film not only became denser, but also grew in the vertical dimension.

4. Discussion

From the SEM examination, it is seen that the initially deposited AuNPs were small, with sizes of about 10–20 nm. This is the mean particle size resulting from the initial precursor gold concentration of 0.5 g/L. As the aerosol droplets travel through the USP reaction tube, they are evaporated, and the gold salt content is reduced with hydrogen gas and densified into AuNPs at a suitable reaction temperature. Such small particles are not stabilised kinetically in the USP flow stream, and have a relatively high surface energy. As the number of AuNPs increases, and the coverage of the glass substrate becomes greater, coalescence and aggregation occur, forming larger individual particles. In the first stage, these larger individual particles are also spherical, but become increasingly irregular as they grow larger.

Evidence of particles shifting and growing together might be the dark spots observed in the advanced AuNP coverage of the sample with 4 h of deposition time, seen in Figures 2iv and 3iv. These dark spots are zones of particle depletion, as the very small AuNPs shifted towards the larger particles, where they aggregated and became a part of the larger particles, or as a part of clusters of primary nanoparticles. With additional deposition time, these zones would again be filled up with AuNPs until the larger particles form an uninterrupted mesh-like structure, and, finally, a continuous Au layer on the glass substrate. Any other potential influence for particle formation was not considered, as the EDX analysis of the AuNPs showed no impurities in the analysed areas.

The samples with deposited AuNPs had a distinctive red transparent colour, and were increasingly less transparent with additional deposition time (supplementary Figure S1). The sample with 4 h of deposition had a more visibly opaque appearance. The ellipsometric measurements of this sample were also not applicable, due to the large scattering of the produced particles. For the other samples, the ellipsometric measurements showed an increasingly denser and thicker effective thickness of the AuNP layers, in accordance with the described particle growth (Table 1). The chosen parameters (gold concentration in the precursor solution, heating temperatures, gas flows) for the given USP system provided adequate control over the AuNP deposition on the glass substrate. It was determined from previous experimental studies [30] that a gold concentration in the precursor solution of 0.5 g/L Au produces relatively small AuNPs, which is beneficial for an evaluation of their LSPR occurrence, as this optical property is more evident in small nanoparticles. Using higher gold concentrations in the precursor solution, or higher gas and material flows, produces larger AuNPs, or a greater number of nanoparticles, which would cover the glass substrate faster, losing some control over the deposition rates in the conducted experiments. A higher temperature also results in higher particle mobility and agglomeration rates of the particles on the glass substrate. The different factors of using various USP parameters would have to be considered in future studies for their optimisation, in order to provide for a quick deposition of a desired size and thickness of the AuNP layer.

Table 1. Effective thickness of the deposited AuNP layers from the ellipsometric measurements.

AuNP Deposition Time	15 Min	30 Min	1 h	4 h
AuNP layer effective thickness from ellipsometric measurements	79 nm	97 nm	110 nm	Not measurable/ large scattering

In order to understand the evolution of the extinction spectra at normal incidence as a function of the deposition time qualitatively (Figure 5) and the effective dielectric function of the AuNP layer (Figure 6), we performed simulations based on the multiple-particle Mie theory, as described elsewhere [36]. In short, the simulations were based in an extension of the Mie theory, in which particles were excited by the incoming radiation and by the field scattered by other particles. We considered 50 nm Au particles embedded in a medium with a refractive index of 1.25 (i.e., the average of an air and glass refractive index) that were distributed randomly in the planar region of 500 nm × 500 nm, as shown schematically in Figure 7 (left). The incoming light was assumed to propagate in the direction perpendicular to the plane of the particles, in order to represent normal incidence measurements. As expected, as the density of the particles increased, the extinction cross-section grew over the whole spectral range where measurements are taken (Figure 7, right panel). Thus, the observed optical response can be explained with an enhanced electromagnetic response between the particles, which can be connected to the increase in particle density, but also by the formation of clusters and irregular structures, as reported in the morphological characterisation.

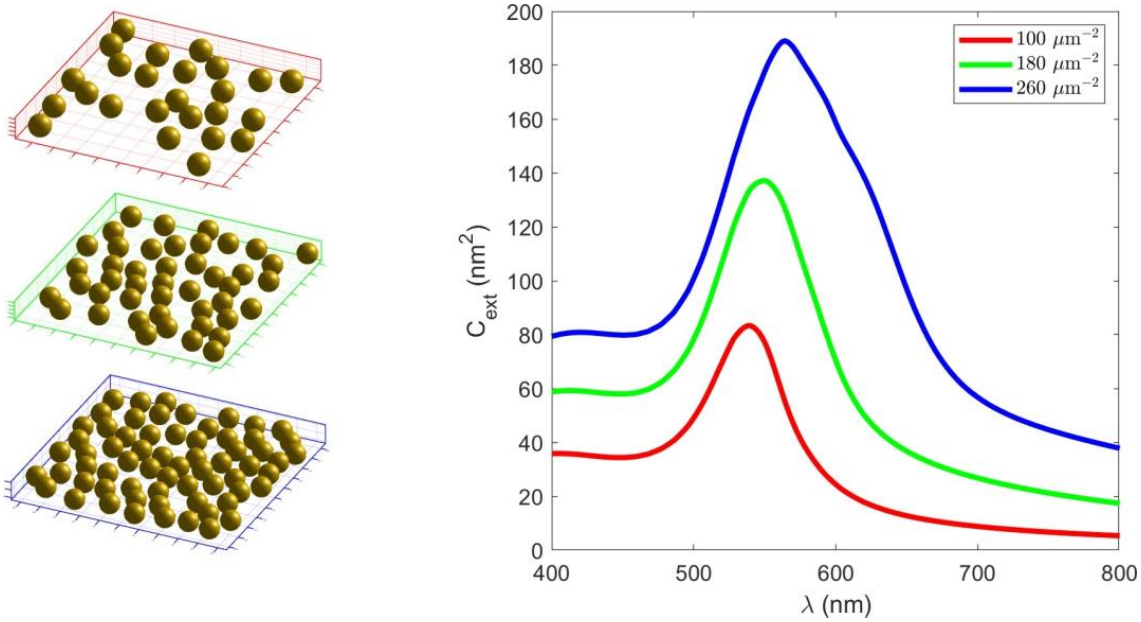

Figure 7. (**left**) Random planar distribution of 25 (**top**), 45 (**middle**) and 65 Au nanoparticles in a 500 nm × 500 nm region. (**right**) Extinction spectra at a normal incidence for the simulated distribution of nanoparticles.

Finally, it should be noted that the effective optical constants of the Au NP layer turned out to be anisotropic. Although such anisotropy can be expected due to the presence of the substrate and the nearly 2-dimensional arrangement of nanoparticles, it is rarely reported in the literature in cases of similar nanoparticle topologies, such as metal island films, or nanoparticles embedded in dielectric layers. The accurate control over particle size and shape enabled by the fabrication methodology results in narrow plasmon resonances that allow for detection of the inherent anisotropic response associated with the film-on-substrate geometry.

5. Conclusions

- The initially deposited AuNPs were small, with sizes of about 10–20 nm. As a higher number of particles were deposited, larger particles were formed and grown through coalescence and aggregation.
- The uniaxial anisotropic model showed better agreement with the ellipsometric measurement data compared to the isotropic model.

- For all AuNP films, a distanced peak at 2.2 eV can be observed in the imaginary part of the dielectric function that corresponds to the LSPR of a single AuNP.
- The perpendicular effective dielectric function showed larger values than the effective parallel dielectric function.
- The effective thickness from the ellipsometry measurements of the AuNP layer for samples deposited at 15, 30 and 60 min were 79, 97 and 110 nm. The AuNP layer deposited after 4 h showed very large depolarisation values due to large scattering, and was not able to be fitted with the used model.
- The higher values of the transmittance and extinction cross-section are related to the longer AuNP deposition times.
- The enhanced electromagnetic response between AuNPs is associated with an increase in their density through the formation of clusters and irregular structures.

In the present work, we have focused on the influence of deposition time on the morphological and optical properties of the films. The effects of other fabrication parameters, such as precursor flow and heater temperature, will be investigated in further studies.

Supplementary Materials: The following supporting information can be downloaded at: https://www.mdpi.com/article/10.3390/surfaces7020023/s1, Figure S1: Appearance of glass substrates with deposited AuNPs, with deposition times of 15 min, 30 min, 1 h and 4 h.

Author Contributions: Conceptualization, J.S.P. and R.R.; methodology, J.S.P., P.M. and Ž.J.; software, J.S.P. and P.M.; validation, R.R. and T.Š.; formal analysis, J.S.P., P.M. and Ž.J.; investigation, R.R. and T.Š.; resources, J.S.P. and R.R.; data curation, J.S.P. and P.M.; writing—original draft preparation, J.S.P., T.Š. and P.M.; writing—review and editing, R.R. and Ž.J.; visualization, J.S.P.; funding acquisition, R.R. All authors have read and agreed to the published version of the manuscript.

Funding: This research was funded by Norway Grants and a corresponding Slovenian contribution within the project: The Recycling of Rapid Antigen LFIA Tests (COVID-19) (LFIA-REC) ATP-150.

Institutional Review Board Statement: Not applicable.

Informed Consent Statement: Not applicable.

Data Availability Statement: The data presented in this study are available on request from the corresponding author.

Conflicts of Interest: Authors Peter Majerič and Rebeka Rudolf were employed by the company Zlatarna Celje d.o.o. The remaining authors declare that the research was conducted in the absence of any commercial or financial relationships that could be construed as a potential conflicts of interest.

References

1. Amendola, V.; Pilot, R.; Frasconi, M.; Maragò, O.M.; Iatì, M.A. Surface Plasmon Resonance in Gold Nanoparticles: A Review. *J. Phys. Condens. Matter* **2017**, *29*, 203002. [CrossRef] [PubMed]
2. Petryayeva, E.; Krull, U.J. Localized Surface Plasmon Resonance: Nanostructures, Bioassays and Biosensing—A Review. *Anal. Chim. Acta* **2011**, *706*, 8–24. [CrossRef]
3. Jain, P.K.; Lee, K.S.; El-Sayed, I.H.; El-Sayed, M.A. Calculated Absorption and Scattering Properties of Gold Nanoparticles of Different Size, Shape, and Composition: Applications in Biological Imaging and Biomedicine. *J. Phys. Chem. B* **2006**, *110*, 7238–7248. [CrossRef] [PubMed]
4. Kelly, K.L.; Coronado, E.; Zhao, L.L.; Schatz, G.C. The Optical Properties of Metal Nanoparticles: The Influence of Size, Shape, and Dielectric Environment. *J. Phys. Chem. B* **2003**, *107*, 668–677. [CrossRef]
5. Hunter, R.J. *Foundations of Colloid Science*; Oxford University Press: New York, NY, USA, 1995; ISBN 9780198505020.
6. Juan, M.L.; Righini, M.; Quidant, R. Plasmon Nano-Optical Tweezers. *Nat. Photonics* **2011**, *5*, 349–356. [CrossRef]
7. Jain, P.K.; Huang, X.; El-Sayed, I.H.; El-Sayed, M.A. Review of Some Interesting Surface Plasmon Resonance-Enhanced Properties of Noble Metal Nanoparticles and Their Applications to Biosystems. *Plasmonics* **2007**, *2*, 107–118. [CrossRef]
8. Philip, A.; Kumar, A.R. The Performance Enhancement of Surface Plasmon Resonance Optical Sensors Using Nanomaterials: A Review. *Coord. Chem. Rev.* **2022**, *458*, 214424. [CrossRef]
9. Chatterjee, S.; Lou, X.-Y.; Liang, F.; Yang, Y.-W. Surface-Functionalized Gold and Silver Nanoparticles for Colorimetric and Fluorescent Sensing of Metal Ions and Biomolecules. *Coord. Chem. Rev.* **2022**, *459*, 214461. [CrossRef]
10. Wang, C.; Yu, C. Detection of Chemical Pollutants in Water Using Gold Nanoparticles as Sensors: A Review. *Rev. Anal. Chem.* **2013**, *32*, 1–14. [CrossRef]

11. Sugunan, A.; Thanachayanont, C.; Dutta, J.; Hilborn, J.G. Heavy-Metal Ion Sensors Using Chitosan-Capped Gold Nanoparticles. *Sci. Technol. Adv. Mater.* **2005**, *6*, 335. [CrossRef]
12. Chah, S.; Hammond, M.R.; Zare, R.N. Gold Nanoparticles as a Colorimetric Sensor for Protein Conformational Changes. *Chem. Biol.* **2005**, *12*, 323–328. [CrossRef] [PubMed]
13. Lv, Z.; He, S.; Wang, Y.; Zhu, X. Noble Metal Nanomaterials for NIR-Triggered Photothermal Therapy in Cancer. *Adv. Healthc. Mater.* **2021**, *10*, 2001806. [CrossRef] [PubMed]
14. Nejabat, M.; Samie, A.; Ramezani, M.; Alibolandi, M.; Abnous, K.; Taghdisi, S.M. An Overview on Gold Nanorods as Versatile Nanoparticles in Cancer Therapy. *J. Control. Release* **2023**, *354*, 221–242. [CrossRef] [PubMed]
15. Khursheed, R.; Dua, K.; Vishwas, S.; Gulati, M.; Jha, N.K.; Aldhafeeri, G.M.; Alanazi, F.G.; Goh, B.H.; Gupta, G.; Paudel, K.R.; et al. Biomedical Applications of Metallic Nanoparticles in Cancer: Current Status and Future Perspectives. *Biomed. Pharmacother.* **2022**, *150*, 112951. [CrossRef] [PubMed]
16. Huang, X.; El-Sayed, M.A. Gold Nanoparticles: Optical Properties and Implementations in Cancer Diagnosis and Photothermal Therapy. *J. Adv. Res.* **2010**, *1*, 13–28. [CrossRef]
17. Que, R.; Shao, M.; Zhuo, S.; Wen, C.; Wang, S.; Lee, S.-T. Highly Reproducible Surface-Enhanced Raman Scattering on a Capillarity-Assisted Gold Nanoparticle Assembly. *Adv. Funct. Mater.* **2011**, *21*, 3337–3343. [CrossRef]
18. Wu, Y.; Ali, M.R.K.; Chen, K.; Fang, N.; El-Sayed, M.A. Gold Nanoparticles in Biological Optical Imaging. *Nano Today* **2019**, *24*, 120–140. [CrossRef]
19. Hou, W.; Cronin, S.B. A Review of Surface Plasmon Resonance-Enhanced Photocatalysis. *Adv. Funct. Mater.* **2013**, *23*, 1612–1619. [CrossRef]
20. Mateo, D.; Cerrillo, J.L.; Durini, S.; Gascon, J. Fundamentals and Applications of Photo-Thermal Catalysis. *Chem. Soc. Rev.* **2021**, *50*, 2173–2210. [CrossRef]
21. Fang, M.; Tan, X.; Liu, Z.; Hu, B.; Wang, X. Recent Progress on Metal-Enhanced Photocatalysis: A Review on the Mechanism. *Research* **2024**, *2021*, 9794329. [CrossRef]
22. Aghlara, H.; Rostami, R.; Maghoul, A.; SalmanOgli, A. Noble Metal Nanoparticle Surface Plasmon Resonance in Absorbing Medium. *Optik* **2015**, *126*, 417–420. [CrossRef]
23. Charles, D.E.; Aherne, D.; Gara, M.; Ledwith, D.M.; Gun'ko, Y.K.; Kelly, J.M.; Blau, W.J.; Brennan-Fournet, M.E. Versatile Solution Phase Triangular Silver Nanoplates for Highly Sensitive Plasmon Resonance Sensing. *ACS Nano* **2010**, *4*, 55–64. [CrossRef]
24. Michaelides, E.E. Brownian Movement and Thermophoresis of Nanoparticles in Liquids. *Int. J. Heat Mass Transf.* **2015**, *81*, 179–187. [CrossRef]
25. Ghasemi, B.; Aminossadati, S.M. Brownian Motion of Nanoparticles in a Triangular Enclosure with Natural Convection. *Int. J. Therm. Sci.* **2010**, *49*, 931–940. [CrossRef]
26. Bhattacharjee, S. DLS and Zeta Potential—What They Are and What They Are Not? *J. Control. Release* **2016**, *235*, 337–351. [CrossRef]
27. Feigin, R.I.; Napper, D.H. Depletion Stabilization and Depletion Flocculation. *J. Colloid Interface Sci.* **1980**, *75*, 525–541. [CrossRef]
28. Trenkenschuh, E.; Friess, W. Freeze-Drying of Nanoparticles: How to Overcome Colloidal Instability by Formulation and Process Optimization. *Eur. J. Pharm. Biopharm.* **2021**, *165*, 345–360. [CrossRef] [PubMed]
29. Beirowski, J.; Inghelbrecht, S.; Arien, A.; Gieseler, H. Freeze Drying of Nanosuspensions, 2: The Role of the Critical Formulation Temperature on Stability of Drug Nanosuspensions and Its Practical Implication on Process Design. *J. Pharm. Sci.* **2011**, *100*, 4471–4481. [CrossRef] [PubMed]
30. Jelen, Ž.; Krajewski, M.; Zupanič, F.; Majerič, P.; Švarc, T.; Anžel, I.; Ekar, J.; Liou, S.-C.; Kubacki, J.; Tokarczyk, M.; et al. Melting Point of Dried Gold Nanoparticles Prepared with Ultrasonic Spray Pyrolysis and Lyophilisation. *Nanotechnol. Rev.* **2023**, *12*, 20220568. [CrossRef]
31. Sancho-Parramon, J.; Okorn, B.; Salamon, K.; Janicki, V. Plasmonic Resonances in Copper Island Films. *Appl. Surf. Sci.* **2019**, *463*, 847–853. [CrossRef]
32. Sancho-Parramon, J.; Janicki, V.; Zorc, H. Tuning the Effective Dielectric Function of Thin Film Metal-Dielectric Composites by Controlling the Deposition Temperature. *J. Nanophotonics* **2011**, *5*, 051805. [CrossRef]
33. Lipovskii, A.A.; Shustova, O.V.; Zhurikhina, V.V.; Svirko, Y. On the Modeling of Spectral Map of Glass-Metal Nanocomposite Optical Nonlinearity. *Opt. Express* **2012**, *20*, 12040–12047. [CrossRef] [PubMed]
34. Hedl, E.; Bregović, V.B.; Rakić, I.Š.; Mandić, Š.; Samec, Ž.; Bergmann, A.; Sancho-Parramon, J. Optical Properties of Annealed Nearly Percolated Au Thin Films. *Opt. Mater.* **2023**, *135*, 113237. [CrossRef]
35. Mendoza-Galván, A.; Järrendahl, K.; Dmitriev, A.; Pakizeh, T.; Käll, M.; Arwin, H. Optical Response of Supported Gold Nanodisks. *Opt. Express* **2011**, *19*, 12093. [CrossRef]
36. Bubaš, M.; Fabijanić, I.; Kenđel, A.; Miljanić, S.; Spadaro, M.C.; Arbiol, J.; Janicki, V.; Sancho-Parramon, J. Unifying Stability and Plasmonic Properties in Hybrid Nanoislands: Au–Ag Synergistic Effects and Application in SERS. *Sens. Actuators B Chem.* **2023**, *380*, 133326. [CrossRef]